Astronomy & Astrophysics manuscript no. emp2_rev_5.0
May 26, 2017

WHT follow-up observations of extremely metal-poor stars identified from SDSS and LAMOST

D. S. Aguado[1,2], J. I. González Hernández[1,2], C. Allende Prieto[1,2], R. Rebolo[1,2,3]

[1] Instituto de Astrofísica de Canarias, Vía Láctea, 38205 La Laguna, Tenerife, Spain

[2] Universidad de La Laguna, Departamento de Astrofísica, 38206 La Laguna, Tenerife, Spain

[3] Consejo Superior de Investigaciones Científicas, 28006 Madrid, Spain

May 26, 2017

ABSTRACT

Aims. We have identified several tens of extremely metal poor star candidates from SDSS and LAMOST, which we follow-up with the 4.2m WHT telescope to confirm their metallicity.
Methods. We follow a robust two-step methodology. We first analyze the SDSS and LAMOST spectra. A first set of stellar parameters is derived from these spectra with the FERRE code, taking advantage of the continuum shape to determine the atmospheric parameters, in particular, the effective temperature. Second, we select interesting targets for follow-up observations, some of them with very low-quality SDSS or LAMOST data. We then obtain and analyze higher-quality medium-resolution spectra obtained with ISIS on the WHT telescope to arrive at a second, more reliable, set of atmospheric parameters. This allows us to derive, with accuracy, the metallicity, and confirm the extremely metal-poor nature in most cases. In this second step we also employ FERRE, but we take a running mean to normalize both the observed and the synthetic spectra, and therefore the final parameters do not rely on having an accurate flux calibration or continuum placement. In order to verify our results we have analyzed with the same tools, and following the same procedure, six well-known metal-poor stars, five of them at [Fe/H]< -4, showing that our methodology is able to get accurate metallicity determinations down to [Fe/H]< -5.0.
Results. The results for these six reference stars give us confidence on the metallicity scale for the rest of the sample. In addition, we present 12 new extremely metal-poor candidates: two stars at [Fe/H] $\simeq -4$, six more in the range $-4 <$ [Fe/H] < -3.5, and four more at $-3.5 <$ [Fe/H] < -3.0.
Conclusions. We conclude that using our improved methodology we can reliably determine metallicities for extremely metal-poor stars with a precision of 0.2 dex from medium-resolution spectroscopy, providing a highly effective way of vetting candidates from lower quality data. Our model spectra, and overall details of the fitting algorithm are made public to facilitate the standardization of the analysis of spectra from the same or similar instruments.

Key words. stars: Population II stars: abundances stars: Population III Galaxy: abundances Galaxy: formation Galaxy: halo

1. Introduction

The oldest stars in the Galactic halo contain information about the early universe after the primordial nucleosynthesis. Such stars are key for understanding how galaxies form, the masses of the first generation of stars, and the early chemical evolution of the Milky Way. The oldest stars are extremely poor in heavy elements and have likely been preceded locally by only one massive star Population III (Frebel et al. 2015). Chemical abundances in extremely metal-poor (EMP) stars (with [Fe/H] < -3), in particular dwarf EMP stars, are needed to study the discrepancy between the primordial lithium abundance obtained from standard Big Bang nucleosynthesis, constrained by the baryonic density inferred from WMAP observations of the CMB (Spergel et al. 2003), and *in situ* atmospheric abundance measurements from old, metal-poor turn-off stars (Spite & Spite 1982; Rebolo et al. 1988; González Hernández et al. 2008; Bonifacio et al. 2009; Sbordone et al. 2012). Unfortunately, very metal-poor stars are extremely rare, with less than ten stars known in the [Fe/H] < -4.5 regime, limiting seriously the number of lithium measurements and detections required to shed light on this problem.

Detailed chemical abundance determinations of EMP stars require high resolution spectroscopy (e.g. Roederer et al. 2014; Frebel & Norris 2015), but the identification of those stars is a difficult task. In the 80's and 90's several different techniques were designed and applied to search for metal poor stars of the Galactic halo using various telescopes equipped with low and medium resolution spectrographs (Beers et al. 1985, 1992; Ryan & Norris 1991; Carney et al. 1996). More recently, the stars with the lowest iron abundances have been discovered from candidates identified in the Hamburg-ESO survey (Christlieb et al. 2002) or the Sloan Digital Sky Survey (SDSS York et al. 2000; Bonifacio et al. 2012). In the last decade, additional stars have been identified by photometric surveys such as the one using the SkyMapper Telescope Keller et al. (2012) or the Pristine Survey (Starkenburg et al. 2017), and spectroscopic surveys such as the Radial Velocity Experiment (RAVE, Fulbright et al. 2010), the Sloan Extension for Galactic Understanding and Exploration (SEGUE,Yanny et al. 2009), or the large Sky Area Multi-Object Fiber Spectroscopic Telescope (LAMOST, Deng et al. 2012).

Table 1. Coordinates and atmospheric parameters for the program stars based in the analysis of the low resolution spectra with FERRE.

Star	g mag	RA h ' "	DEC ° ' "	$T_{\rm eff}$ K	$\log g$ cm s^{-2}	[Fe/H]	[C/Fe]	< S/N >[a]	survey
SDSS J015131+163944	18.9	01:51:31.2	+16:39:44.98	5917	3.9	-3.6	1.3	19	BOSS
SDSS J030444+391021	17.8	03:04:44.97	+39:10:21.17	5918	4.9	-3.7	0.3	29	SEGUE
SDSS J105519+232234	17.8	10:55:19.28	+23:22:34.03	6448	4.9	-4.2	-0.3	32	BOSS
SDSS J132917+542027	14.9	13:29:17.34	+54:20:27.52	5876	0.5	-4.0	–	47	LAMOST
SDSS J134157+513534	15.4	13:41:57.97	+51:35:34.08	6011	1.5	-4.9	–	35	LAMOST
SDSS J134338+484426	12.6	13:43:38.66	+48:44:26.48	5390	1.0	-3.7	0.7	56	SEGUE
SDSS J152202+305526	16.6	15:22:02.09	+30:55:26.29	5500	0.6	-4.1	–	37	SEGUE
SDSS J173329+332941	18.9	17:33:29.32	+33:29:41.94	6448	4.5	-4.2	0.7	21	SEGUE
SDSS J200513−104503	17.0	20:05:13.48	-10:45:03.21	6488	4.4	-3.7	-0.7	45	SEGUE
SDSS J202109+601605	17.9	20:21:09.01	+60:16:05.33	5834	3.3	-3.4	0.4	20	SEGUE
SDSS J204524+150825	16.7	20:45:24.03	+15:08:25.46	5069	2.4	-3.6	0.0	39	SEGUE
SDSS J231027+231003	17.3	23:10:27.16	+23:10:03.43	6188	4.1	-4.0	–	33	SEGUE
SDSS J222505+164322	18.0	22:25:05.97	+16:43:22.52	5378	1.0	-3.7	0.9	24	BOSS

Notes. [a] Signal-no-noise ratio have been calculated as average of the SDSS or LAMOST entire spectrum

Extremely metal-poor stars tend to be located at large distances. For these stars, spectroscopic surveys do not usually provide spectra with sufficient quality, and therefore, it is critical to vet candidates with additional observations with higher quality.

In this work, we follow a two-step methodology to identify new extremely metal-poor stars:

- Perform an improved analysis of SDSS and LAMOST to select EMP candidates,
- Carry out follow-up observations of a subsample which allow us to check their stellar parameters, metallicities and carbon abundances.

The paper is organized as follows. In Section 2 we explain how candidates are selected. Section 3 is devoted to the follow-up observations and data reduction. Section 4 describes in detail how the analysis is carried out, including tests using well-known metal-poor stars (Section 4.1). We then discuss our carbon abundance determination from low- and medium-resolution spectra (Section 8). Finally, Section 5 summarizes our results and conclusions.

2. Low spectral resolution analysis and target selection

We have analyzed the low-resolution spectra of more than 2.5 million targets from three different surveys: the Baryonic Oscillations Spectroscopic Survey (BOSS, Eisenstein et al. 2011; Dawson et al. 2013), SEGUE (Yanny et al. 2009) and LAMOST (Deng et al. 2012). The analysis of the stars from these surveys has been performed with FERRE [1] (Allende Prieto et al. 2006), which allows us to derive the main stellar parameters, effective temperature $T_{\rm eff}$, and surface gravity $\log g$, together with the metallicity [Fe/H] [2], and carbon abundance [C/Fe] (see Aguado et al. 2016, for further details). As a result of the extremely-low metal abundances of our targets, iron transitions are not detected, either individually or even as blended features, in medium resolution spectra. We usually measure only the Ca II resonance lines and use them as a proxy for the overall metal abundance of the stars, assuming the typical iron-to-calcium ratio found in metal-poor stars [Fe/H]=[Ca/H]−0.4.

We have analyzed about 1,700,000 (∼1,500,000 stars) spectra from LAMOST, 740,000 (∼660,000 stars) from SEGUE and 340,000 (∼300,000 stars) from BOSS. A database with all candidates at [Fe/H]< −3.5 has been built containing ∼ 500 objects with a first set of stellar properties ($T_{\rm eff}$, $\log g$, [Fe/H], [C/Fe]). However, this first selection still contains many outliers and non reliable fits. We re-evaluate the goodness of fit measuring the χ^2 in a limited spectral region around the Balmer lines. This method prevents false positives even at low signal-to-noise ratios (S/N<20). Finally a visual inspection of the spectra and their best fittings has been carried out, to skim the best several tens of candidates. The stars that have passed this selection are then scheduled for observations at medium-resolution and much higher signal-to-noise ratio. Table 1 shows the derived parameters of the final sample analyzed in this work. Visual inspection helps us to detect promising candidates. The two LAMOST objects discussed below are a good example where visual inspection was critical. In addition to these stars, we have chosen some of the most metal-poor stars known ([Fe/H]< −4.0), with published determinations from high-resolution spectroscopic data, in order to test our methodology.

3. Observations and data reduction

The second step in our methodology makes use of follow-up medium resolution spectroscopy obtained with the ISIS (Jorden 1990) spectrograph on the 4.2-m William Herschel Telescope (WHT), at the Observatorio del Roque de los Muchachos (La Palma, Spain). We used the R600B and R600R gratings, the GG495 filter in the red arm, and the default dichroic (5300 Å). The mean FWHM resolution with a one-arcsecond slit was R∼ 2400 in the blue arm and R∼ 5200 in the red arm. More details are provided in Aguado et al. (2016). The observations were carried out over the course of five observing runs; Run I: Dec 31 - Jan 2 (3 nights), 2015; II: February 5-8 (4 nights), 2015; III: August 14-18 (5 nights), 2015; IV: May 1-2 (2 nights), 2016 and V: July 29 - 31 (3 nights), 2016. A standard data reduction (bias substraction, flat-fielding and wavelength calibration, using

[1] FERRE is available from http://github.com/callendeprieto/ferre

[2] We use the bracket notation for reporting chemical abundances: [a/b]= $\log \frac{N(a)}{N(b)} - \log \frac{N(a)}{N(b)}_{\odot}$, where N(x) represents number density of nuclei of the element x.

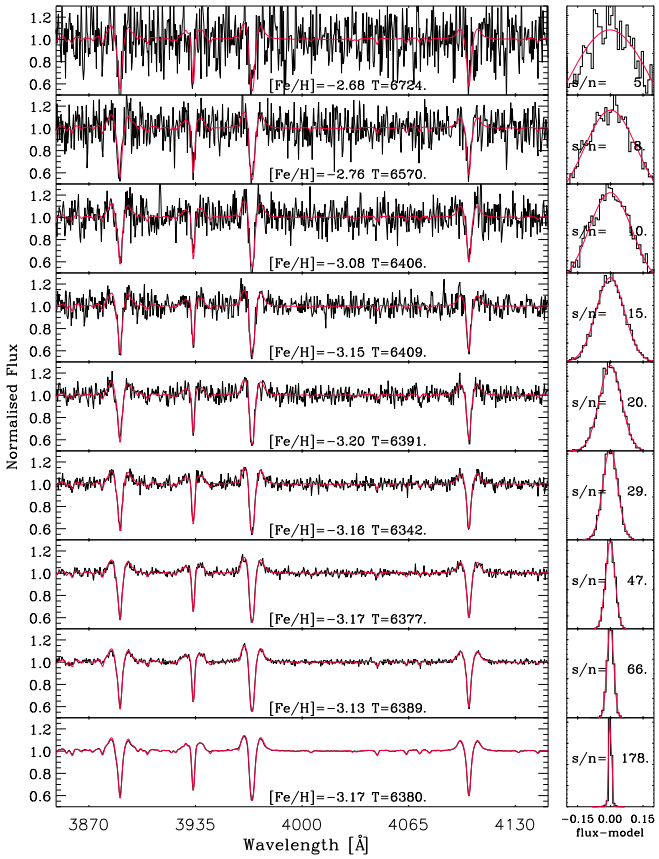

Fig. 1. Left panel: medium resolution ISIS spectrum of G64-12 with different levels of added poisson noise (black lines) and the best fit computed by FERRE (red line). Right panel: the Gaussian distribution of the signal-to-noise ratio computed on the residuals from subtracting the best-fitting model to the observed spectrum.

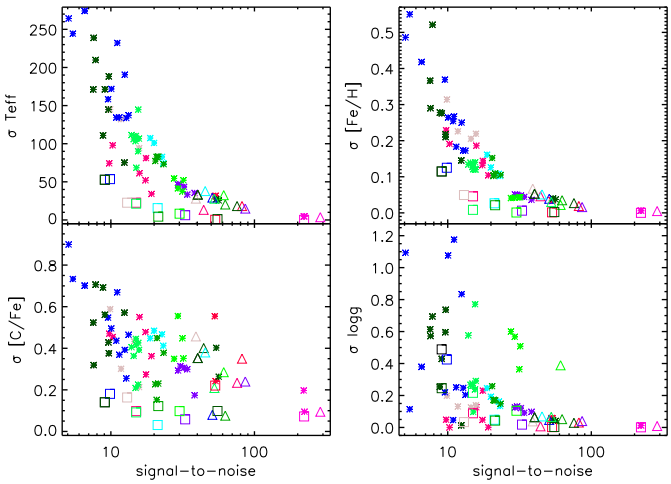

Fig. 2. Random errors derived by FERRE as a function of the signal-to-noise ratio for individual and combined exposures. Each color represents a different star presented in this paper. The triangles correspond to the combined spectra and asterisks to the individual exposures, with random errors estimated by FERRE and given in Table 2. The squares show the dispersion in the parameters derived from individual exposures, showed at the mean value of their signal-to-noise ratio.

CuNe + CuAr lamps) was performed with the *onespec* package in IRAF[3] (Tody 1993).

High resolution spectra of well-known metal-poor stars were extracted from the ESO archive[4] and obtained with the Ultraviolet and Visual Echelle Spectrograph (UVES, Dekker et al. 2000) at the VLT. The spectral range of these data is 3300-4500 Å and the resolving power is about 47,000. The spectra were reduced using the automatic UVES pipeline (Ballester et al. 2000), offered to the community through the ESO Science Archive Facility.

4. Analysis and discussion

In order to derive the stellar parameters and chemical abundances a grid of synthetic spectra has been computed with the ASSϵT code (Koesterke et al. 2008), which uses the Barklem codes (Barklem et al. 2000a,b) for describing the broadening of Balmer lines. The grid resembles the one used by Allende Prieto et al. (2014), with some differences described below, and it is provided, ready to be used with FERRE as an electronic table. The model atmospheres have been computed with the same Kurucz codes and the strategies described by Mészáros et al. (2012). The abundance of α−elements has been fixed to [α/Fe] = +0.4, and the limits of the grid are $-6 \leq$ [Fe/H] ≤ -2; $-1 \leq$ [C/Fe] ≤ 5, 4750 K $\leq T_{\rm eff} \leq$ 7000 K and $1.0 \leq \log g \leq 5.0$, assuming a microturbulence of 2 km s^{-1}. We search for the best fit using FERRE deriving simultaneously the main three atmospheric parameters and the carbon abundance.

Interstellar reddening and the instrument response distort the intrinsic shape of the stellar spectra. To minimize systematic differences between the synthetic spectra and the observations, we work with continuum-normalized fluxes. Both the observed and synthetic spectra are normalized using a running-mean filter with a width of 30 pixels (about 10 Å). Although the precision in the derived parameters has been found to be very sensitive to the normalization scheme, our tests show that when no reliable information on the shape spectral energy distribution is available, the running-mean filter offers very good performance. With this modification we are able to retrieve $T_{\rm eff}$ and $\log g$ information from ISIS spectra.

In order to check how robust the FERRE results are, we carry out a series of consistency tests, adding random noise with a Normal distribution to an observed spectrum of the metal-poor star G64-12. The results are illustrated in Fig. 1 and described below. We find that FERRE is able to recover the original set of parameters from high S/N values down to S/N = 15 when the derived solution begins to drift away from the expected solution. This is consistent with the results obtained by Allende Prieto et al. (2014) for SDSS spectroscopy.

[3] IRAF is distributed by the National Optical Astronomy Observatory, which is operated by the Association of Universities for Research in Astronomy (AURA) under cooperative agreement with the National Science Foundation

[4] Based on data from the ESO Science Archive Facility

We use observations of well-known metal-poor stars to test our methodology. The comparison between the literature metallicities from high resolution analyses and those we obtain using medium resolution spectroscopy indicates our approach works quite well. Nonetheless, our methodology does not allow us to separate the Ca II K spectral lines from the star from the ISM contributions that are not resolved in the ISIS spectra. We describe below tests in which re-analyze the original UVES spectra (See Section 4.1) of several objects after smoothing to understand the effect of having lower spectral resolution.

FERRE is able to derive internal uncertainties in several ways. After testing extensively in our ISIS spectra, we find that the best option is to inject noise using a Normal distribution to the observed spectra multiple times, and search for the best-fitting parameters. Such Monte-Carlo simulations are performed 50 times for each observed spectrum. The dispersion in the derived parameters is adopted as a measurement of the internal uncertainty on these parameters in our analysis. In addition to the final combined spectra for each target, we have analyzed in the same fashion each individual exposure. Fig. 2 shows the relationship between our derived internal random uncertainties and the signal-to-noise ratio. The uncertainties on the final combined spectra follow the same trend found in the analysis of individual exposures. The only giant star in the sample, J2045+1508, shows a higher uncertainty in its surface gravity determination, as expected (see Table 2). From these tests, we conclude that our random errors are consistently and reliably determined, with the exception of the [C/Fe] abundance ratios, for which we tend to underestimate the random uncertainties, given that the dispersion from individual estimates of this parameter is larger than the random error from individual exposures. This is particularly relevant at [C/Fe]$<$ 1.0 dex.

In addition to random errors, other sources of systematic uncertainty can affect our results. Stellar effective temperatures are not easy to determine accurately (see, e.g., Sbordone et al. 2010). We adopt a 100 K uncertainty following the comparison between photometric and spectroscopic methods by Yong et al. (2004). In addition, the stellar isochrones depicted in Fig. 7 suggest that systematic 0.3 − 0.5 dex error could be present in our spectroscopic gravities (see §4.2 and 5). From these comparisons, we decided to adopt a systematic uncertainty in surface gravity of 0.5 dex. The error bars shown for the data in Fig. 7 are the quadratic combination of our estimated random and systematic uncertainties. We adopt 0.1 dex metallicity error, according to the comparisons between our results and those in the high-resolution analyzes in the literature, but warn that much larger systematic uncertainties could be present due to departures from LTE and hydrostatic equilibrium (see, Shchukina et al. (2005); Nordlander et al. (2017) and references therein) which could add up to 0.8-0.9 dex. Based on other works (see section 8) we estimate that our derived carbon abundances could have a systematic uncertainty of about 0.3 dex. In Table 3, we show the carbon abundances for well-know metal-poor stars whose uncertainties have been computed by adding in quadrature the random error and the adopted systematic error.

4.1. Well-known metal-poor stars

4.1.1. G64-12

Aoki et al. (2006) observed G64-12 with High Dispersion Spectrograph (HDS) at the Subaru telescope, and derived its main atmospheric parameters $T_{\rm eff} = 6390 \pm 100\,K$, $\log g = 4.4 \pm 0.3$ and [Fe/H] $= -3.2 \pm 0.1$. We obtained with ISIS/WHT a high-quality spectrum (S/N$\sim$ 300) of this object, and derived a set of parameters in excellent agreement with those from Aoki et al. (2006): $T_{\rm eff} = 6377 \pm 104\,K$, $\log g = 4.8 \pm 0.7$ and [Fe/H] $= -3.2 \pm 0.2$.

4.1.2. SDSS J1313−0019

There is an open debate about the metallicity of this object, discovered by Allende Prieto et al. (2015) using a low-resolution spectrum from the BOSS project (Eisenstein et al. 2011; Dawson et al. 2013). Allende Prieto et al. (2015) derived the following set of parameters: $T_{\rm eff} = 5300 \pm 50\,K$, $\log g = 3.0 \pm 0.2$, [Fe/H] $= -4.3 \pm 0.1$ and [C/Fe] $= 2.5 \pm 0.1$. This temperature reproduces both the local continuum slope and the shape of the Balmer lines in the BOSS spectrum of the star. Shortly after the discovery, Frebel et al. (2015) obtained a high resolution ($R \sim 35,000$) spectrum with the MIKE spectrograph at the Magellan-Clay telescope. Their adopted effective temperature and surface gravity are $T_{\rm eff} = 5200 \pm 150\,K$ and $\log g = 2.6 \pm 0.7$. They measured 37 Fe I lines (Fe II features were not detected) and estimated a metallicity of [Fe/H] $= -5.00 \pm 0.28$ and [C/Fe] $= 2.96 \pm 0.28$.

A high-S/N medium-resolution spectrum of J1313−0019 was obtained as part of our WHT program. Fig. 3 shows the entire spectrum, and the best-fitting from the FERRE analysis. We derive $T_{\rm eff} = 5525 \pm 106\,K$, $\log g = 3.6 \pm 0.5$, [Fe/H] $= -4.7 \pm 0.2$ and [C/Fe] $= 2.8 \pm 0.30$. Our derived metallicity is in between those by Allende Prieto et al. (2015) and Frebel et al. (2015), but closer to the determination by Frebel et al. (2015). Using carbon-enhanced model atmospheres, consistent with the high [C/Fe] ratio adopted in the spectral synthesis, does not introduce significant changes in the derived values. The difference between our analysis and that in Allende Prieto et al. (2015) is partly explained by the fact we assume [α/H] $= 0.4$ while the authors derived [α/H] $= 0.2 \pm 0.1$.

We have checked that if we impose in the FERRE analysis the same effective temperature and surface gravity adopted by Frebel et al. (2015) ($T_{\rm eff} = 5200$ and $\log g = 2.6$), we recover a metallicity and carbon abundance of [Fe/H] $= -4.9 \pm 0.2$ and [C/Fe] $= 2.7 \pm 0.3$, respectively. The adoption of an effective temperature 300 K cooler by Frebel et al. (2015) is responsible for an offset of about 0.2 dex in metallicity. Since our value of $T_{\rm eff}$ (See Table 2) is mostly based on fitting of all Balmer lines available in the spectrum we consider it reliable.

4.1.3. HE 0233−0343

This star was studied by Hansen et al. (2014) using high-resolution spectra acquired with UVES on the VLT, and it is one of the rare stars at such low metallicity where the lithium abundance has been measured, A(Li) = 1.77. These objects are key for understanding the cosmological Li problem (e.g. Asplund et al. 2006; Bonifacio et al. 2007; González Hernández et al. 2008). Our effective temperature determination, $T_{\rm eff} = 6150 \pm 103\,K$, is consistent with that proposed by Hansen et al. (2014), $T_{\rm eff} = 6100 \pm 100\,K$. They assumed an age of 10 Gyr to infer a surface gravity of $\log g = 3.4 \pm 0.3$ from isochrones, while we derive $\log g = 4.9 \pm 0.7$ from the ISIS spectrum.

Calcium ISM absorption is clearly visible in the UVES spectrum of this star, but it is not resolved at the ISIS resolution (See Fig. 4). The presence of an unresolved ISM contribution biases our metallicity determination from FERRE to [Fe/H] $= -4.0 \pm 0.1$, while Hansen et al. (2014) derive [Fe/H] $= -4.7 \pm 0.2$. To check the consistency of the high- and medium-resolution re-

sults, we have smoothed the UVES spectrum to the ISIS resolution and re-analyzed it, arriving at the same result as for the ISIS data: $T_{\rm eff}$ = 6207 K; $\log g$ = 4.9 and [Fe/H] = −4.0, as illustrated in Fig. 4.

4.1.4. SDSS J1029+1729

The star SDSS J1029+1729 has no carbon (or nitrogen) detected, which makes it the most metal-poor star ever discovered (Caffau et al. 2011, 2012). This rare object challenges theoretical calculations that predict no low-mass stars can form at very low metallicities. Using UVES with a resolving power $R \sim 38000$ (Caffau et al. 2012) derived the following set of parameters: $T_{\rm eff} = 5811 \pm 150$ K, $\log g = 4.0 \pm 0.5$ and [Fe/H] = -4.9 ± 0.2. Our analysis of the medium-resolution ISIS spectra arrives at $T_{\rm eff} = 5845 \pm 105$ K, $\log g = 5.0 \pm 0.8$ and [Fe/H] = -4.4 ± 0.2. Following a similar argument as given in Section 4.1.3, the difference in metallicity is associated to the calcium ISM contribution (See Fig. 4). This is demonstrated by degrading the UVES spectrum to the resolution of the ISIS data. Such analysis gives a result that is fully consistent with the one from the ISIS spectrum: $T_{\rm eff}$ = 5867 K, $\log g$ = 5.0 and [Fe/H] = −4.5.

4.1.5. HE 1327−2326

The study of this star is complicated due to the complex structure of the calcium ISM features, and the extraordinary amount of carbon ([C/Fe] = 4.26, Frebel et al. 2005; Aoki et al. 2006) present in the stellar atmosphere (see Fig. 4). The parameters from Aoki et al. (2006) from a high-resolution UVES spectrum are $T_{\rm eff} = 6180 \pm 100$ K; $\log g = 3.7 \pm 0.3$ and [Fe/H] = -5.6 ± 0.1 while FERRE returns $T_{\rm eff} = 6150 \pm 102$ K, $\log g = 4.3 \pm 0.7$ and [Fe/H] = -4.8 ± 0.2 from the medium-resolution ISIS spectrum. We display in Fig. 4 the original UVES observation, the same data smoothed to the resolution of ISIS, and the ISIS spectrum.

The UVES spectrum resolves multiple ISM features, while ISIS only uncovers some of the blue components so that the FERRE analysis of the ISIS spectrum returns a higher metallicity. Once more, the smoothed spectrum solution is consistent with our own medium-resolution ISIS values: $T_{\rm eff}$ = 6119 K; $\log g$ = 4.3 and [Fe/H] = −4.9. The use of medium resolution data leads inevitably to a biased metallicity due to unresolved ISM calcium absorption.

4.1.6. SDSS J1442−0015

The S/N ratio of this spectrum is the lowest in our sample since it is one of the faintest metal-poor star in the [Fe/H] < −4.0 regime. Even so, the original set parameters derived from UVES spectroscopy by Caffau et al. (2013), $T_{\rm eff} = 5850 \pm 150$ K, $\log g = 4.0 \pm 0.5$ and [Fe/H] = -4.1 ± 0.2, are in fair agreement with our determinations from ISIS data: $T_{\rm eff} = 6036 \pm 102$ K, $\log g = 4.9 \pm 0.5$ and [Fe/H] = -4.4 ± 0.2.

The spectrum of J1442−0015 shows clearly an ISM contribution to the observed calcium absorption, but such component is already resolved in the ISIS data (See Fig. 4). The adopted effective temperature by Caffau et al. (2013), slightly lower than our FERRE estimate, should lead to a difference of at least ∼0.4 dex between both metallicity determinations but in the opposite direction to what we find. In addition, our analysis of the UVES spectrum smoothed to the resolution of ISIS provides a $T_{\rm eff}$ = 6167 K, $\log g$ = 4.9 and [Fe/H] = −4.2, consistent with the results from ISIS.

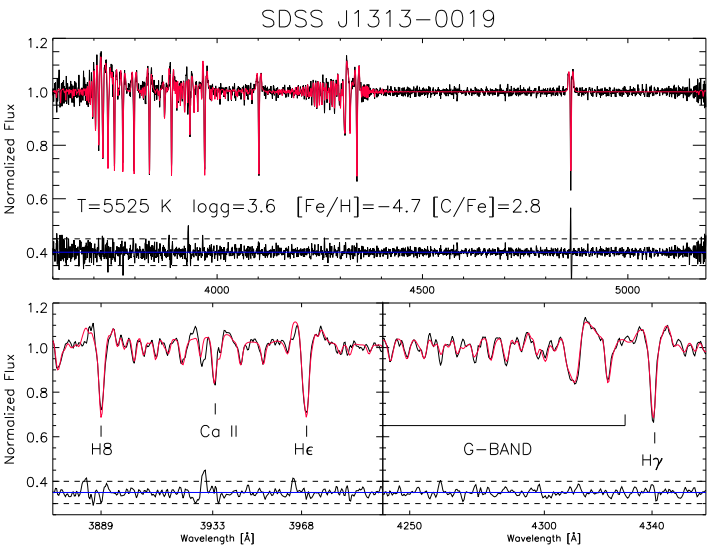

Fig. 3. Top panel: The blue ISIS J1313−0019 spectrum (black line) and the best fit computed with FERRE (red line) with the residuals (black line over blue reference). The derived stellar parameters and carbon abundance are shown. Bottom panel: A detail of the Ca II H-K and the g-band spectral region.

4.2. A new set of extremely metal-poor stars

Following the same methodology in Section 4.1, we have analyzed spectra from the ISIS instrument for a sample of metal-poor stars candidates identified from SDSS and LAMOST. The mean S/N of these spectra is around 75, so we expect the FERRE results to be reliable. Our effective temperatures are trustworthy, since we have been able to recover it for several well-known metal-poor stars whose metallicities are consistent with the literature values. In addition, the derived metallicities by FERRE are also reliable and consistent with the results obtained from the analysis of SDSS spectra (see Allende Prieto et al. 2014, for further details). Only our surface gravities appear to be subject to a systematic error of about 0.5 dex. This is in contrast to the small random uncertainties we derive for our stellar parameters, and surface gravity in particular (§4): less than 0.1 dex at S/N∼ 50.

Fig. 7 shows DARMOUTH isochrones [5], HB, and AGB tracks compared to the stellar parameters derived using FERRE on the ISIS spectra and their derived error bars. Our mean uncertainty in the metallicity determination is 0.12 dex. whereas the mean uncertainty in $T_{\rm eff}$ is 103 K.

The mean metallicity difference between our first metallicity estimates from SDSS/LAMOST spectra and the second we obtain from higher quality ISIS spectra is 0.31 dex with a standard deviation of 0.20 dex. In this computation we have excluded the stars J134157+513534 and J132917+542027, since the metallicity differences for them are much larger. The LAMOST spectra of these stars show several artifacts which do not allow us to perform a correct continuum normalization with our running-mean algorithm, and consequently we are not deriving robust parameters from those data. However, our ISIS spectra have significantly higher quality, S/N∼ 82 and 76, and we finally derive a reliable metallicity for both stars, [Fe/H]= −2.7 and [Fe/H]= −3.5

[5] The Dartmouth Stellar Evolution Program (DSEP) is available from www.stellar.dartmouth.edu

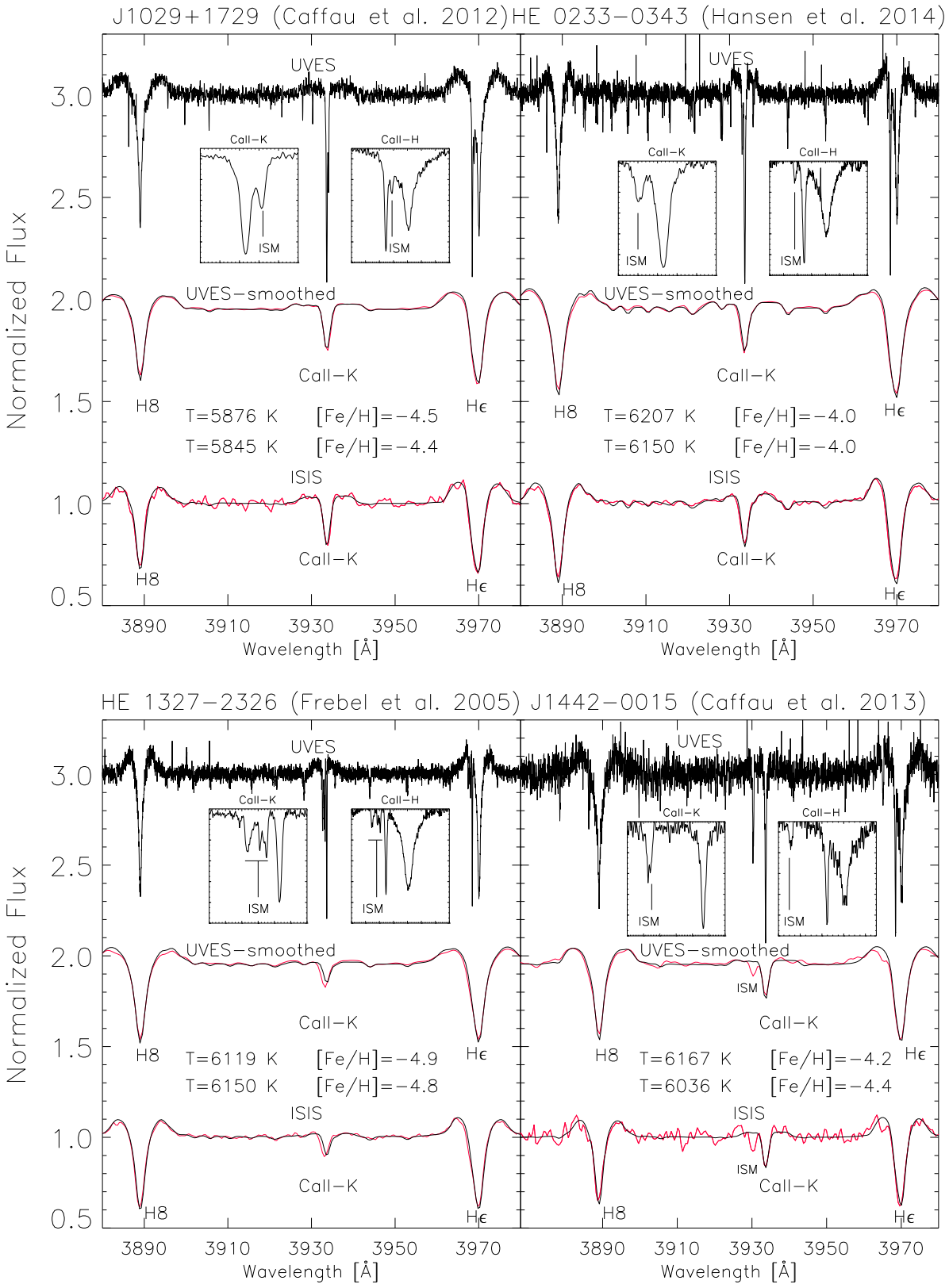

Fig. 4. Spectra in the range of the Ca II lines for four well-known metal-poor stars. *from top to bottom*, UVES, UVES smoothed to ISIS resolution and ISIS spectra (black line) and the best medium resolution fit (red line). Details of the calcium lines in the UVES spectra are included in the insets together with the effective temperature and metallicity derived with FERRE for UVES-smoothed and ISIS spectra.

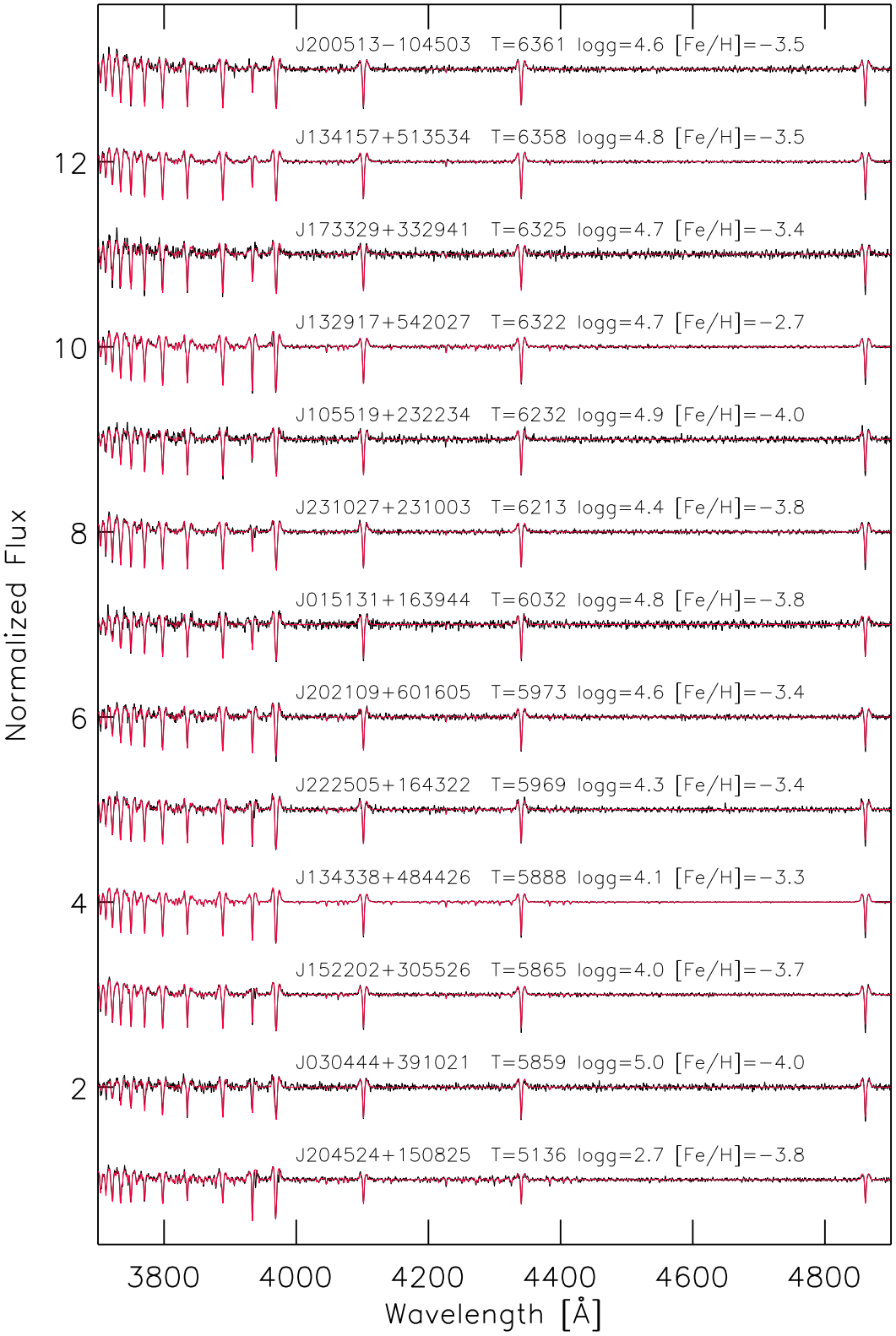

Fig. 5. ISIS/WHT blue arm spectra (3700 Å-4900 Å) for the full sample (black line) and the best fit calculated with FERRE (red line). The main stellar parameters are also displayed.

Table 2. The stellar parameters and main results obtained from ISIS spectra.

Star	N_{exp} 1800 s	$\langle S/N \rangle^a$	T_{eff} [K]	ΔT_{eff} [K]	log g [cm s^{-2}]	Δ log g [cm s^{-2}]	[Fe/H]	Δ[Fe/H]	[C/Fe]	Δ[C/Fe]
SDSS J015131+163944	10	40	6032	33	4.8	0.07	-3.8	0.05	1.3	0.35
SDSS J030444+391021	6	44	5859	13	5.0	0.01	-4.0	0.05	<0.7	–
SDSS J105519+232234	4	39	6232	28	4.9	0.03	-4.0	0.07	<0.7	–
SDSS J132917+542027	2	82	6322	18	4.7	0.03	-2.7	0.02	<0.7	–
SDSS J134157+513534	2	76	6358	18	4.8	0.02	-3.5	0.03	<0.7	–
SDSS J134338+484426	2	287	5888	4	4.1	0.01	-3.3	0.01	0.8	0.09
SDSS J152202+305526	6	86	5865	15	4.0	0.04	-3.7	0.02	0.8	0.24
SDSS J173329+332941	12	51	6325	29	4.7	0.05	-3.4	0.04	1.8	0.08
SDSS J200513−104503	4	45	6361	38	4.6	0.06	-3.5	0.05	<0.7	–
SDSS J202109+601605	9	52	5973	28	4.7	0.07	-3.4	0.03	0.7	0.20
SDSS J204524+150825	4	61	5136	32	2.7	0.38	-3.8	0.02	0.3	0.28
SDSS J231027+231003	7	62	6213	20	4.4	0.05	-3.8	0.04	1.5	0.08
SDSS J222505+164322	6	50	5969	21	4.3	0.06	-3.4	0.04	0.8	0.39
HE 0233−0343[(1)]	6	65	6150	16	4.9	0.02	-4.0	0.03	2.2	0.15
SDSS J1029+1729[(2)]	6	69	5845	13	5.0	0.01	-4.4	0.04	0.4[b]	0.75
SDSS J1313−0019[(3,4)]	7	66	5525	17	3.6	0.05	-4.7	0.03	2.8	0.03
HE 1327−2326[(5,6)]	2	133	6101	11	4.3	0.02	-4.8	0.03	3.0	0.03
G64−12[(6)]	2	321	6377	5	4.8	0.01	-3.2	0.01	0.4[b]	0.15
SDSS J1442−0015[(7)]	7	42	6036	31	4.9	0.08	-4.4	0.01	0.5[b]	0.47

Notes. [a] Signal-to-noise ratios have been calculated as the average of S/N values for the entire SDSS spectrum. [b] Values below our limit detection.

Notes. Δ is the internal uncertainty of the parameters derived with FERRE.

Notes. (1) =Hansen et al. (2014); (2) =Caffau et al. (2012); (3) =Allende Prieto et al. (2015); (4) =Frebel et al. (2015); (5) =Frebel et al. (2005); (6) =Aoki et al. (2006); (7) =Caffau et al. (2013)

respectively. In Fig. 6 we compare the results summarized in Table 2 with those from low-resolution analysis (Table 1). In addition, we have re-analyzed the stars studied in Aguado et al. (2016) with the improved methodology presented in this work. We obtain a slightly higher dispersion for candidates with lower quality spectra.

Our analysis uncovers two objects (J0304+3910 and J1055+2322) at [Fe/H]$\simeq -4.0$ and six more at $-3.5 \geq$[Fe/H]> -4.0, in the domain of the extremely metal-poor stars, and most of them appear to be dwarfs at log $g \geq 4.0$. A deeper study of this sample using high-resolution spectroscopy would provide abundances for additional elements, helping to constrain the nature of the stars and the early chemical evolution of the Galaxy.

4.3. Carbon abundances

Carbon-enhanced metal-poor (CEMP) stars are defined by Beers & Christlieb (2005) as stars having [C/Fe]$\geq +1.0$. The fraction of CEMP/EMP stars increases as metallicity decreases. Deriving reliable carbon abundances in metal-poor stars using medium resolution spectroscopy is not always possible (Bonifacio et al. 2015). For the well-know EMP sample studied in Section 4.1 we recover carbon abundances compatible with the literature values for three CEMP stars: SDSS J1313−0019, HE 1327−2326 and HE 0233−0343 (see Table 3).

Fig. 8 shows the carbon abundances derived from ISIS spectra for the targets studied in this work, together with those from Aguado et al. (2016), with the improved methodology, and other CEMP stars from the literature. The data suggest the lower the metallicity, the larger the carbon enhancement, as expected (see e.g. Lee et al. (2013)). Our ability to measure carbon abundances decreases as the effective temperature of the star increases due to CH dissociation. Empirically, to measure carbon abundances at the level of [C/Fe]$\geq +0.5$ the star should

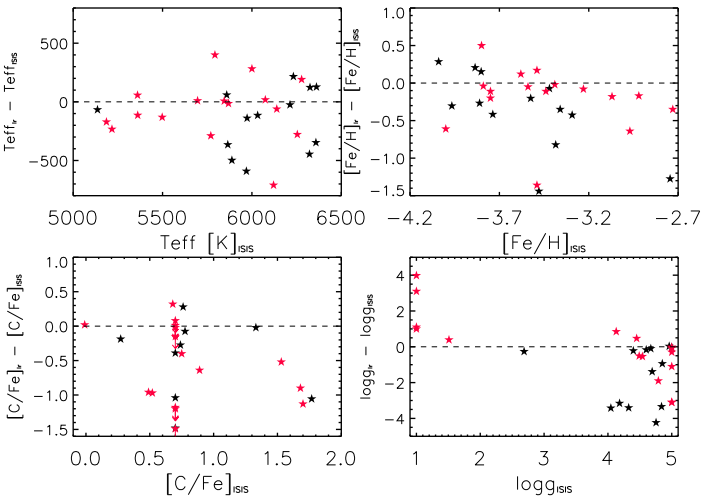

Fig. 6. Comparison between the main stellar parameters derived by FERRE from low-resolution (SDSS and LAMOST) data and from ISIS spectra. Objects included in this work sample appear as black filled stars while objects from our previous work Aguado et al. (2016) are red filled stars.

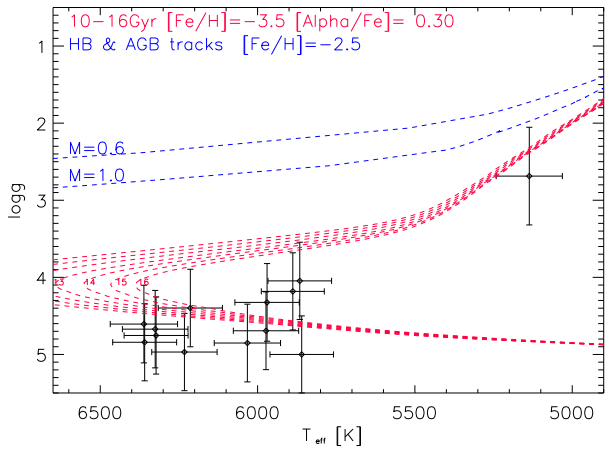

Fig. 7. DARMOUTH isochrones for [Fe/H] = −3.5 and different ages from 16 to 10 Gyr (red dashed lines), blue dashed lines are HB and AGB theoretical tracks for [Fe/H] = −2.5 for two different relative masses (M = 0.6 and M = 1.0). The black diamonds represent the stars of this work and its internal uncertainties derived with the FERRE code.

Table 3. Carbon abundances results.

star	Bibliography UVES/MIKE A(C)(Δ)	This work ISIS A(C)(Δ)
HE 0233−0343	7.18(0.24)	6.7(0.3)
SDSS J1029+1729	n.d.	4.5(0.8)
SDSS J1313−0019	6.46(0.28)	6.6(0.3)
HE 1327−2326	7.20(0.2)	6.7(0.3)
G64−12	5.8(0.2)	5.7(0.4)
SDSS J1442−0015	n.d.	4.6(0.6)

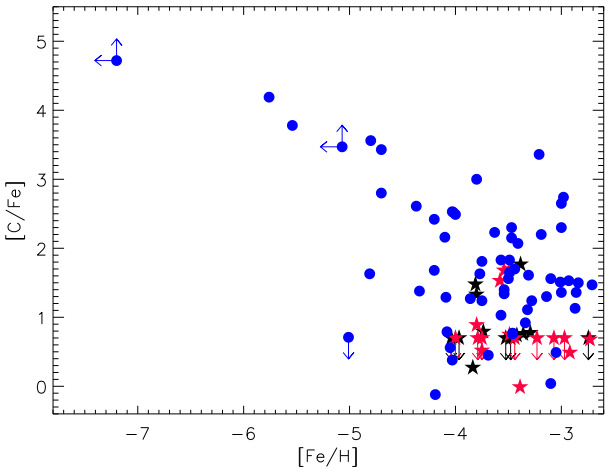

Fig. 8. Carbon over iron versus metallicities of stars presented in this work (black filled stars) and those from Aguado et al. (2016) (red filled stars) analyzed with the improved methodology, together with stars from the literature (Sivarani et al. 2006; Yong et al. 2013; Frebel et al. 2005, 2006; Caffau et al. 2014; Allende Prieto et al. 2015) represented by blue filled circles.

have a $T_{\rm eff}$ ∼ 5500/5700 K. Moreover, if the effective temperature lies at ∼ 5000/5100 K we are able to measure carbon at [C/Fe]≥ +0.0. In addition, a S/N of at least 30 is required to derive reliable carbon abundances. Table 2 summarizes our results, and shows that our sample includes at least three confirmed CEMP stars: SDSS J0151+1639, SDSS J1733+3329 and SDSS J2310+1210 with [Fe/H]= −3.8, −3.4 and −3.8, respectively, in perfect agreement with the statistics by Cohen & Huang (2009); Bonifacio et al. (2015). In addition, an additional five stars appear to be very close to our detection limit [C/Fe]∼ +0.7 − 0.8.

5. Conclusions

We have demonstrated that our methodology to identify metal-poor stars using low- and medium-resolution spectroscopy is effective. We have been able to scrutinize more than 2.5 million spectra from SDSS and LAMOST to identify extremely-metal poor stars candidates which we have followed-up with significantly higher signal-to-noise ratio and slightly higher resolution ISIS observations. Our success identifying metal-poor candidates is quite high, with only one star, J1329+5420, at [Fe/H]> −3.

The use of the FERRE code and a custom grid of synthetic spectra allows us to derive simultaneously the atmospheric parameters and the carbon abundance, improving our values from SDSS or LAMOST. We have shown that FERRE can be used efficiently on extremely metal-poor stars. We make our tools publicly available to facilitate the cross-calibration of results from other teams. Our method offers an excellent way to identify and analyze CEMP star candidates without the need for high resolution spectroscopy. We have presented a new EMP sample and reliable determinations of their metallicities and carbon abundances.

These stars, especially the two at [Fe/H]< −4.0, are good candidates for follow-up high-resolution observations. This domain is sparsely populated, with less than 30 stars known, and of high interest for investigating the early chemical evolution of the Galaxy. The fact that we have used a grid of synthetic spectra including carbon as a free parameter not only in the synthesis but in the model atmospheres helps us to detect promising extremely metal-poor stellar candidates and derive their carbon abundances when [C/Fe]> 0.7 − 1.0 and S/N> 30/40, and even lower carbon enhancements and/or S/N values if the star is colder than 5500 K.

We have included in our work several well-known metal-poor stars previously analyzed in the literature. A study of these objects is useful to check for systematic differences due to multiple analysis methodologies. Our results shown that we are able to recover the effective temperature with an uncertainty of about 100 K and the metallicity within 0.2 dex. In addition, the comparison of our parameters with model isochrones suggests that our surface gravities have a systematic uncertainty of about 0.5 dex. Our study confirms as well that we are able to recover the carbon abundance for CEMP stars using medium-resolution spectra.

Future work should include observations at higher resolution of the most interesting extremely metal-poor stars identified in this paper, to study in detail their chemical abundance patterns.

Acknowledgements. DA is thankful to the Spanish Ministry of Economy and Competitiveness (MINECO) for financial support received in the form of a Severo-Ochoa PhD fellowship, within the Severo-Ochoa International PhD Program. DA, CAP, JIGH, and RR acknowledge the Spanish ministry project MINECO AYA2014-56359-P. JIGH acknowledges financial support from the Spanish Ministry of Economy and Competitiveness (MINECO) under the 2013 Ramón y Cajal program MINECO RYC-2013-14875. This paper is based on observations made with the William Herschel Telescope, operated by the Isaac

Newton Group at the Observatorio del Roque de los Muchachos, La Palma, Spain, of the Instituto de Astrofísica de Canarias. We thank the ING staff members for their assistance and efficiency during the four observing runs in visitor mode.
The author thankfully acknowledges the technical expertise and assistance provided by the Spanish Supercomputing Network (Red Espanola de Supercomputacion), as well as the computer resources used: the LaPalma Supercomputer, located at the Instituto de Astrofisica de Canarias.

References

Aguado, D. S., Allende Prieto, C., González Hernández, J. I., et al. 2016, A&A, 593, A10
Allende Prieto, C., Beers, T. C., Wilhelm, R., et al. 2006, ApJ, 636, 804
Allende Prieto, C., Fernández-Alvar, E., Aguado, D. S., et al. 2015, A&A, 579, A98
Allende Prieto, C., Fernández-Alvar, E., Schlesinger, K. J., et al. 2014, A&A, 568, A7
Aoki, W., Frebel, A., Christlieb, N., et al. 2006, ApJ, 639, 897
Asplund, M., Lambert, D. L., Nissen, P. E., Primas, F., & Smith, V. V. 2006, ApJ, 644, 229
Ballester, P., Modigliani, A., Boitquin, O., et al. 2000, The Messenger, 101, 31
Barklem, P. S., Piskunov, N., & O'Mara, B. J. 2000a, A&AS, 142, 467
Barklem, P. S., Piskunov, N., & O'Mara, B. J. 2000b, A&A, 363, 1091
Beers, T. C. & Christlieb, N. 2005, Highlights of Astronomy, 13, 579
Beers, T. C., Preston, G. W., & Shectman, S. A. 1985, AJ, 90, 2089
Beers, T. C., Preston, G. W., & Shectman, S. A. 1992, AJ, 103, 1987
Bonifacio, P., Caffau, E., Spite, M., et al. 2015, A&A, 579, A28
Bonifacio, P., Molaro, P., Sivarani, T., et al. 2007, A&A, 462, 851
Bonifacio, P., Sbordone, L., Caffau, E., et al. 2012, A&A, 542, A87
Bonifacio, P., Spite, M., Cayrel, R., et al. 2009, A&A, 501, 519
Caffau, E., Bonifacio, P., François, P., et al. 2011, Nature, 477, 67
Caffau, E., Bonifacio, P., François, P., et al. 2013, A&A, 560, A15
Caffau, E., Bonifacio, P., François, P., et al. 2012, A&A, 542, A51
Caffau, E., Sbordone, L., Bonifacio, P., et al. 2014, Mem. Soc. Astron. Italiana, 85, 222
Carney, B. W., Laird, J. B., Latham, D. W., & Aguilar, L. A. 1996, AJ, 112, 668
Christlieb, N., Wisotzki, L., & Graßhoff, G. 2002, A&A, 391, 397
Cohen, J. G. & Huang, W. 2009, ApJ, 701, 1053
Dawson, K. S., Schlegel, D. J., Ahn, C. P., et al. 2013, AJ, 145, 10
Dekker, H., D'Odorico, S., Kaufer, A., Delabre, B., & Kotzlowski, H. 2000, in Proc. SPIE, Vol. 4008, Optical and IR Telescope Instrumentation and Detectors, ed. M. Iye & A. F. Moorwood, 534–545
Deng, L.-C., Newberg, H. J., Liu, C., et al. 2012, Research in Astronomy and Astrophysics, 12, 735
Eisenstein, D. J., Weinberg, D. H., Agol, E., et al. 2011, AJ, 142, 72
Frebel, A., Aoki, W., Christlieb, N., et al. 2005, Nature, 434, 871
Frebel, A., Chiti, A., Ji, A. P., Jacobson, H. R., & Placco, V. M. 2015, ApJ, 810, L27
Frebel, A., Christlieb, N., Norris, J. E., et al. 2006, ApJ, 652, 1585
Frebel, A. & Norris, J. E. 2015, ARA&A, 53, 631
Fulbright, J. P., Wyse, R. F. G., Ruchti, G. R., et al. 2010, ApJ, 724, L104
González Hernández, J. I., Caballero, J. A., Rebolo, R., et al. 2008, A&A, 490, 1135
Hansen, T., Hansen, C. J., Christlieb, N., et al. 2014, ApJ, 787, 162
Jorden, P. R. 1990, in Society of Photo-Optical Instrumentation Engineers (SPIE) Conference Series, Vol. 1235, Instrumentation in Astronomy VII, ed. D. L. Crawford, 790–798
Keller, S. C., Skymapper Team, & Aegis Team. 2012, in Astronomical Society of the Pacific Conference Series, Vol. 458, Galactic Archaeology: Near-Field Cosmology and the Formation of the Milky Way, ed. W. Aoki, M. Ishigaki, T. Suda, T. Tsujimoto, & N. Arimoto, 409
Koesterke, L., Allende Prieto, C., & Lambert, D. L. 2008, ApJ, 680, 764
Lee, Y. S., Beers, T. C., Masseron, T., et al. 2013, AJ, 146, 132
Mészáros, S., Allende Prieto, C., Edvardsson, B., et al. 2012, AJ, 144, 120
Nordlander, T., Amarsi, A. M., Lind, K., et al. 2017, A&A, 597, A6
Rebolo, R., Beckman, J. E., & Molaro, P. 1988, A&A, 192, 192
Roederer, I. U., Preston, G. W., Thompson, I. B., et al. 2014, AJ, 147, 136
Ryan, S. G. & Norris, J. E. 1991, AJ, 101, 1835
Sbordone, L., Bonifacio, P., & Caffau, E. 2012, Memorie della Societa Astronomica Italiana Supplementi, 22, 29
Sbordone, L., Bonifacio, P., Caffau, E., et al. 2010, A&A, 522, A26
Shchukina, N. G., Trujillo Bueno, J., & Asplund, M. 2005, ApJ, 618, 939
Sivarani, T., Beers, T. C., Bonifacio, P., et al. 2006, A&A, 459, 125
Spergel, D. N., Verde, L., Peiris, H. V., et al. 2003, ApJS, 148, 175
Spite, M. & Spite, F. 1982, Nature, 297, 483
Tody, D. 1993, in Astronomical Society of the Pacific Conference Series, Vol. 52, Astronomical Data Analysis Software and Systems II, ed. R. J. Hanisch, R. J. V. Brissenden, & J. Barnes, 173
Yanny, B., Rockosi, C., Newberg, H. J., et al. 2009, AJ, 137, 4377
Yong, D., Lambert, D. L., Allende Prieto, C., & Paulson, D. B. 2004, ApJ, 603, 697
Yong, D., Norris, J. E., Bessell, M. S., et al. 2013, ApJ, 762, 26
York, D. G., Adelman, J., Anderson, Jr., J. E., et al. 2000, AJ, 120, 1579